THE CUBESAT MISSION FUTURE: A PRELIMINARY ANALYSIS TO VALIDATE THE ON-BOARD AUTONOMOUS ORBIT DETERMINATION

Carmine Buonagura[(1)], Salvatore Borgia[(1)], Mattia Pugliatti[(1)], Alessandro Morselli[(1)], Francesco Topputo[(1)], Filippo Corradino[(2)], Pierluigi Visconti[(2)], Luca Deva[(2)], Alberto Fedele[(3)], Giuseppe Leccese[(3)], Silvia Natalucci[(3)]

[(1)]*Politecnico di Milano, Via La Masa 34, 20156 Milano, Italy, +39-0223997157, {carmine.buonagura, salvatore.borgia, mattia.pugliatti, alessandro.morselli, francesco.topputo}@polimi.it*

[(2)]*Tyvak International, Via Orvieto 19, 10149 Torino, Italy, +39-01119116070, {filippo.corradino, pierluigi.visconti, luca.deva}@tyvak.eu*

[(3)]*Italian Space Agency (ASI), Via del Politecnico snc, 00133, Roma, Italy, +39-068567360, {alberto.fedele, giuseppe.leccese, silvia.natalucci}@asi.it*

ABSTRACT

FUTURE is a 6U CubeSat whose aim is to make advancements in the autonomy of spacecraft in providing position knowledge and reducing reliance on operators and ground support services and facilities. The mission aims at flying a set of sensors on a singe satellite in LEO, and use the data generated to feed different artificial intelligence algorithms to identify features on the Earth's surface and to elaborate position knowledge. The outcome of the project will be directed toward future applications beyond LEO, such as in missions about planets and moons, enhancing autonomous operation and navigation in the proximity of different celestial bodies. The purpose of this work is to provide an updated overview of the FUTURE mission, and to illustrate the architecture and some preliminary results of the autonomous navigation strategy.

1 INTRODUCTION

The Fully aUtonomous feaTUre Recognition planetary Explorer (FUTURE) is a Low Earth Orbit (LEO) nanosatellite mission that has recently concluded Phase A, whose aim is to demonstrate the capability of autonomously determining its orbit exploiting only visual observations [6], [8]–[11], without relying on radiometric measurements or on Global Navigation Satellite Systems (GNSS) [5]. Such approach represents a paradigm shift in how deep-space missions are navigated. Currently, deep-space navigation relies mostly on either radiometric tracking or ground-based orbit determination [16] which requires dedicated antenna networks such as the European Space Tracking Station (ESTRACK) of ESA and the Deep Space Network (DSN) of NASA. While radiometric measurements can provide accurate orbit determination, they require frequent communications with the ground stations, increasing the costs of operations. FUTURE as in-orbit demonstrator could validate this innovative navigation concept with beneficial impacts on beyond-LEO missions: more spacecraft autonomy will reduce spacecraft-ground interactions, hence minimizing the need for operators and ground support, and in turn the operations costs. FUTURE will fly a set of optical sensors on a single satellite and will use the acquired data to feed artificial intelligence algorithms to detect time invariant features of the Earth's surface, such as lakes and coastlines. These data are then processed on-board to

generate positional inputs that the navigation filter will process to determine the satellite state in terms of both position and velocity. Furthermore, opportunistic observations with other celestial objects can be carried on concurrently to validate alternative autonomous navigation techniques using different sets of measurements. Being in Earth orbit, it will be possible to assess the orbit determination accuracy achievable on-board with artificial intelligence and filtering techniques by taking as a reference the satellite state estimation performed by means of GALILEO/GNSS measurements.
This work presents the outcomes of the Phase A study of FUTURE, focusing on the navigation filter preliminary architecture, the on-board navigation performance assessment, as well as relevant mission analysis studies. The paper is organized into three main parts: the first part will thoroughly describe the FUTURE mission and its innovative goals. In the second part, the considered Sun-Synchronous operational Orbit (SSO) will be defined. Coverage analysis will be performed to understand when it is possible to acquire meaningful terrestrial feature images and take advantage of the autonomous navigation algorithm. Maximum eclipse times and flyover times of oceans or polar regions will be determined to understand the worst-case scenario in terms of free filter propagation. The visibility of the Moon and planets throughout the mission will be established to understand the time windows in which opportunistic scenarios can be exploited. Subsequently, the navigation filter preliminary architecture is described and some results are discussed. In Phase A, a Hybrid Extended Kalman Filter (HEKF) [1], [4] has been employed. As the filter shall operate with different set of range measurement (features and Moon observations) two different operative scenarios are described and analyzed. The nominal scenario is represented by the natural features of the planet, through which accuracies of few hundred meters can be achieved [7]. The opportunistic scenario is instead exploiting the Moon, with lower accuracies due to its large distance. This kind of navigation could be carried out during periods when the satellite flies over the oceans or polar regions, where it is not possible to perform feature-based navigation. Finally, some future developments of the navigation filter during phase B are given together with some hints of the potential applications of the proposed technology. In particular, it will be analyzed how it could enhance autonomous operation and navigation around other planets and moons by exploiting their morphological features and how the opportunistic scenario could be exploited to complement periods during which relevant morphological features are not present on the ground or when the main attractor is in eclipse.
FUTURE is one of the 20 missions funded by ASI under the ALCOR program [15], aimed at placing Italy in a condition of consolidated leadership in the nano and microsatellite sector. The FUTURE consortium is composed of entities and institutions from Italy. Tyvak International serves as the prime contractor, managing the entire program and providing mission development, system integration and verification, launch coordination, and mission operations support. The DART team at Politecnico di Milano is responsible for the mission analysis and for the design, verification, and validation of the navigation filter solution. ALTEC is in charge of the ground segment design and spacecraft operations. AIKO oversees the development of artificial intelligence-based image processing algorithms.

2 MISSION OVERVIEW

FUTURE is a LEO nanosatellite mission to in-orbit demonstrate the capability of determining the spacecraft orbit only with visual observation, without relying on ranging measurements, or on the GNSS positioning systems. Given the current state of the art, this project is aimed to enhance autonomous navigation capabilities in LEO via natural and artificial features on the surface of the Earth. In particular, the project is expected to prove an innovative low-cost and autonomous navigation technique for LEO applications. Furthermore, opportunistic observations with other celestial objects can be carried on concurrently in order to validate autonomous navigation techniques spanning different scales. Technology transfer is key for this mission: the outcome of the project can be directed

for future applications beyond LEO, such as in missions about planets, moons, and deep space, so enhancing autonomous operation and navigation in the proximity of different celestial bodies. The solution will make use of state of art automation algorithms, sensors, processing units and software solutions to obtain position and velocity information.
The project case study is a 6U CubeSat orbiting in a circular LEO orbit at about 600 km altitude with two navigation cameras differing in field of view (FOV). The main camera will have a nadir pointing to Earth to detect macro-size surface features. From such an altitude, the swath of a 16 deg FOV camera is about 170 km, which would be ideal to detect bodies of water such as rivers, lakes, coastlines, and regional geological features. The other camera will have a narrow 3 deg FOV pointing toward the Moon and other celestial bodies. The latter camera is used to obtain opportunistic observations in a way that does not interfere with the main camera pointing toward Earth. These kinds of observations could be planned during the eclipse periods to complement the main ones. The proposed mission consists of a Tyvak 6U nanosatellite based on the Trestles platform[1] and is designed for a nominal mission duration of 6 months.
This period can be divided in 4 different phases: 1) Launch and Early Orbit Phase (LEOP), 2) Commissioning phase, for the carrier and the payloads, 3) Nominal operations phase, 4) Decommissioning phase and disposal.

The main goal of the project is to increase the onboard autonomous optical navigation capabilities for resource and cost-constrained CubeSat missions. This will be achieved by fulfilling the objectives reported in Table 1. To achieve these goals, the responsibilities of the consortium members are clearly

Table 1: FUTURE mission objectives.

Mission objective	**Text**
OBJ 1	Identification of key requirements and constraints for autonomous optical navigation techniques to be embedded into CubeSat satellite missions.
OBJ 2	Design of robust, small latency, autonomous optical navigation technologies applicable at different scales.
OBJ 3	In-Orbit validation of these techniques using Galileo/GNSS as reference measurements.
OBJ 4	Demonstrate technology transfer capabilities from LEO to deep-space applications.

defined: the payload hardware will be provided by Tyvak and all software and algorithms by AIKO and the Politecnico di Milano. Finally, a combination of Tyvak's and ALTEC's ground infrastructure will be used to operate the spacecraft.

3 ORBIT ANALYSIS AND STUDIES

The preliminary operative orbit has been selected to be a SSO, with an altitude of about 600 km to be conservative in terms of ground resolution and to be compliant with the end-of-life constraints. The orbit Keplerian elements have been selected to guarantee a weekly repeat ground-track and a 10:30 – 22:30 SSO, which represents an orbit crossing the ascending node at 10:30 local time. As a result, the inclination i and the initial right ascension of the ascending node (RAAN) have been selected equal to 97.9 deg and 60.5 deg, respectively. The preliminary operative orbit is depicted in Figure 1 and the nominal orbit main orbital parameters are shown in Table 2.

[1] `https://www.tyvak.eu/platforms/` Last access: 10 May 2023

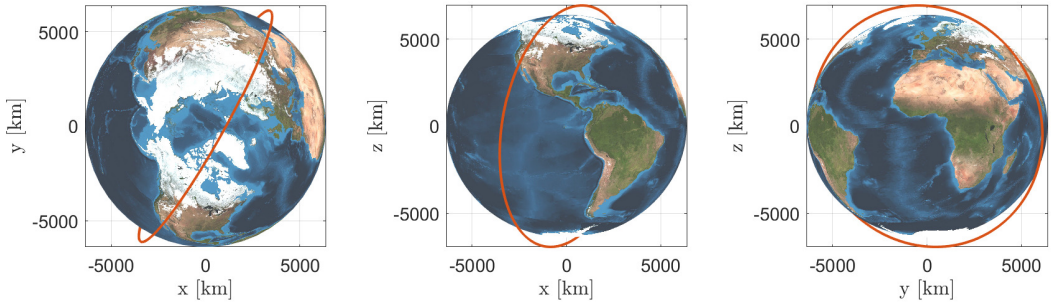

Figure 1: Preliminary sun-synchronous operative orbit for the FUTURE mission. The red line represents one revolution of the orbit.

Table 2: Nominal orbit main orbital parameters.

a [km]	**e [-]**	**i [deg]**	**Ω [deg]**	**T [min]**
6976.7	0	97.9	60.5	96.6583

Tyvak Trestles is the platform considered, whose main parameters are reported in Table 3. Where C_d and C_r are the drag and reflectivity coefficients respectively. The force models considered in the simulation are:

- 30x30 spherical harmonic model
- Spherical Solar Radiation Pressure (SRP) model
- MSISE90 atmosphere model
- Point mass perturbations from the Sun and the Moon

Moreover, it is important to note that the SRP area has been set equal to the maximum possible area of the satellite, including the solar panels, to be in the most conservative scenario possible.

Table 3: FUTURE satellite main parameters.

Parameter	**Value**	**Units**
Mass	14.5	kg
SRP Area	0.5032	m^2
Drag Area	0.0368	m^2
C_d	2.2	-
C_r	1.85	-

3.1 Terrain visibility

An important parameter for mission success is to maximize terrain visibility in order to perform navigation with artificial intelligence (AI) algorithms. For this reason, an analysis of the coverage of ground areas was performed to understand their visibility percentage over a time window of 7 days. Given the repeated ground track, the analysis of the first week holds for the rest of the duration of the nominal mission. To accomplish this task, the following approach was considered: the main continents and islands were treated as polygons, and a punctual analysis was performed to understand

when the satellite's longitude and latitude coordinates (nadir pointing) lie within these polygons. The result is that the percentage of visible ground areas in this time frame is 23.71% for the nominal operational orbit considered. A further analysis was carried out to assess the percentage of land visible under daylight conditions only. To do this, the previously calculated visibility conditions were further elaborated. Indeed, daylight conditions of a longitude-latitude coordinate were evaluated by ensuring that the angle between the Earth-Satellite vector and the Earth-Sun vector was less than 90 deg. This second analysis showed that 13.56% of the 7-day trajectory can be exploited for AI navigation under daylight conditions. This analysis has been performed at other three launch dates to assess the change in terrain visibility due to seasonal variations. Specifically, the other three dates considered are close to the autumn equinox and winter solstice in 2024, and the spring equinox in 2025. Table 4 summarizes the percentage of terrain visibility considering both night and daylight conditions as well as only daylight ones. As expected, the percentage of visible terrain in spring results to be higher than in the fall and winter seasons because the northern hemisphere (where the large majority of emerged land is located) is more illuminated.

Table 4: Time percentage of a 7-day repeat cycle with terrain visibility.

Launch date	**Lighting condition**	**Visibility percentage [%]**
14 June 2024	Day and night	23.7103
	Day	13.5615
20 September 2024	Day and night	23.7103
	Day	11.0020
20 December 2024	Day and night	23.7103
	Day	10.1290
21 March 2025	Day and night	23.7103
	Day	12.8075

The coverage analysis was performed for several orbits corresponding to an Ascending Node Local Time (LTAN) ranging from 08:00:00 to 16:00:00, equivalent to RAAN values spanning from 23 to 143 deg. Table 5 shows the time percentage of the 7-day repeat cycle during which the terrain below the spacecraft can be acquired. In this table, the selected nominal orbit is highlighted. Figure 2 shows the variation of the time percentage with terrain visibility in daylight conditions as a function of the initial value of the right ascension of the ascending node.

Table 5: Time percentage of a 7-day repeat cycle with terrain visibility for different RAAN values.

RAAN [deg]	**LTAN [-]**	**Day and night visibility [%]**	**Day visibility [%]**
23	08:00:00	23.7698	15.3174
35	08:48:00	23.8294	14.4296
47	09:36:00	23.8790	13.9137
59	10:24:00	23.7649	13.5863
60.5	10:30:00	23.7202	13.5615
71	11:12:00	23.7351	13.5813
83	12:00:00	23.8244	13.9038
95	12:48:00	23.9037	14.2609
107	13:36:00	23.8046	14.7619
119	14:24:00	23.8145	15.3869
131	15:12:00	23.7946	16.3442
143	16:00:00	23.8641	17.6438

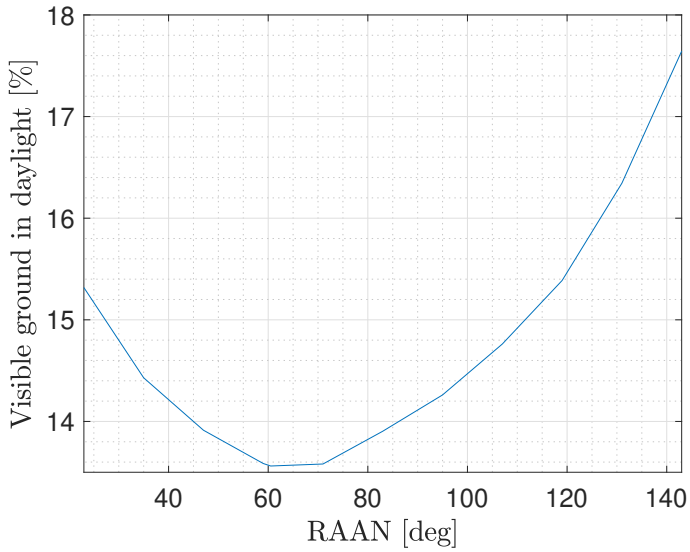

Figure 2: Time percentage of terrain visibility in daylight conditions as functions of RAAN considering a launch date corresponding to June 14, 2024 and a 7-day simulation analysis.

It is clear that the time percentage with terrain visibility is minimum for a RAAN value of 60 deg, corresponding to an ascending node local time around 10:30:00. It must be emphasized that the analysis performed is preliminary and the result is valid only near the selected launch date (14th June 2024). In a 6-months simulation, seasonal variability implies a lengthening or shortening of the day duration and thus variations in the results obtained. In the operation period considered for our simulations, the Northern Hemisphere, where most of the dry lands are located, is illuminated for longer periods, which implies a higher percentage of daytime visibility of emerged areas. This analysis also allowed the estimation of the maximum time spent over land areas and over areas where it is not possible to have observations (gaps). Two conditions were analyzed and results are summarized in Table 6. The first is purely geometric, so the maximum consecutive visibility times of land (target), and of ocean and sea areas in a 7-day simulation could be directly computed: in the first case this period is equal to 18.5 minutes, while the second one is 94.5 minutes. This implies that there are some entire orbits for which the satellite cannot observe land areas. The second instead takes also lighting conditions into account, hence eclipses are considered. The duration of the time interval in which the target can be seen remains the same, but at the same time, an increase in consecutive observations were terrestrial regions cannot be acquired increases up to 180.5 minutes. It must be noted that this value is greater than the sum of the worst eclipse duration time (34.6 min) and the maximum consecutive time of oceans visibility (94.5 min), which would sum up to 129.6 minutes. This happens because there is an unlucky combinations where the oceans are observed in daylight and the terrestrial areas are eclipses. This is the worst-case condition that will be considered to evaluate the free propagation performance of the navigation filter. In this scenario the navigation filter shall be able of maintain adequate estimation accuracy.

Table 6: Maximum visibility time window of land and ocean areas.

	Max target visibility [min]	**Max observations gap [min]**
Geometrical	18.5	94.5
Light conditions	18.5	180.5

3.2 Opportunistic scenarios

Opportunistic scenarios are planned for the FUTURE mission to test the platform's ability to recover its state in terms of position and velocity by exploiting celestial bodies other than Earth. These scenarios are useful for testing spacecraft navigation capabilities in deep space missions. The main opportunistic mission scenario is to perform lunar relative navigation. Then another nice to have possibility would be to use visible planets to retrieve information about the satellite's position and velocity. To perform this type of navigation, it is necessary to understand when the Moon and planets can be detected. For this reason, an approach has been designed to check whether the Moon and planets are visible during the satellite's operational lifetime. This is done by calculating the satellite-body vector and checking if there are intersections with the Earth, modeled as a sphere of constant radius equal to 6378 km. If there are no intersections of the vector with the Earth, the body is geometrically visible in the Field Of View (FOV) of the camera. If intersections occur, it is necessary to calculate the direction of the intersections with respect to the direction of the vector. If the intersections are at a negative distance (opposite to the satellite pointing direction), it means that the Earth is not occulting the body. If either intersection has a positive distance from the satellite's position, it means that the Earth is between the satellite and the body, causing its occultation. The geometric visibility of the body does not imply its detectability by the camera sensor. Regarding the Moon, an important parameter is the Sun phase angle φ, which is defined as the angle between satellite-body-Sun (see Figure 3), while for planets their magnitude must be considered. Two other important parameters for the detectability of bodies are the exclusion angles of the Earth and Sun, which represent the angle below which scattered light from the Earth's limb, or the Sun does not allow the detectability of other bodies and may cause damage to the sensor. Their value is assumed to be 30 deg (half cone) for the Sun, and 25 deg for the Earth's limb. These values will be consolidated in the later stages of the mission.

3.2.1 Moon visibility

The detectability of the Moon is driven by the value of the Sun phase angle. Indeed, to have enough light from it and successfully apply image processing algorithms, it is necessary that this angle is below 120 deg. In this condition less than half of the Moon is illuminated. Figure 3 shows an intuitive representation of the geometric conditions for the Moon visibility and the Sun phase angle ϕ that enable its detection.

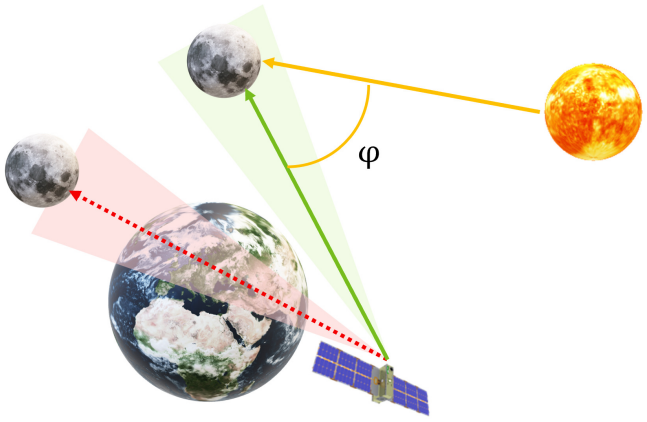

Figure 3: Sun phase angle and conditions for Moon geometrical visibility.

The analysis performed computes the percentage of Moon detectability per orbit in a 6-month simulation. As can be seen in Figure 4, there are orbits in which the satellite-Moon- Sun configuration is

such that the Moon cannot be seen. During a synodic month, corresponding to one Moon revolution around the Earth (29 d 12 h 44 min and 2.9 s), the Moon can be detected for around 20 consecutive days during at least 50% of the orbital period. A no visibility period of about 10 days repeats periodically since the Moon is in full shadow when observed by the satellite.

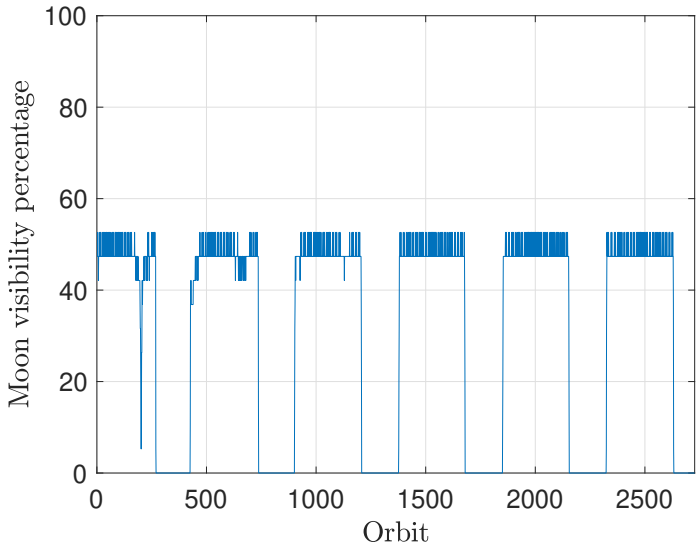

Figure 4: Moon visibility percentage per orbit.

These ten-day gaps in which the Moon is not visible make this scenario only opportunistic and not complementary to navigation based on land areas. This result has driven the concept of operations of the mission, indeed, since it is not possible to observe the Moon under all possible conditions, but huge gaps are present, the baseline of the mission will be observations of land areas. The observation of the Moon will be decoupled from the evaluation of the state (position and velocity) of the satellite for navigation purposes but will only be demonstrative to evaluate the performance of the navigation algorithm to retrieve the state of the satellite from the observations of a celestial object.

3.2.2 Planets visibility

The detectability of planets strongly depends on their magnitude. In particular, for a typical CubeSat sensor, planets with a magnitude less than 5 can be detected [12], [17]. A simple analysis was carried out to compute the number of visible planets per orbit. In particular, the planets considered are Mercury, Venus, Mars, Jupiter, and Saturn. From Figure 5a it is possible to see the results achieved. Moreover, in Figure 5b it is shown which planets are visible during the 6-month simulation. It is clear that the results are strongly affected by the launch date selected. Mercury is the only planet that is not visible throughout the entire duration of the mission because of its proximity to the Sun.
The planets visibility analysis has been provided here to simply characterize the frequency of the observations during the nominal mission duration. These observations are not intended to be processed by the navigation filter given their lower accuracy, that is at least one order of magnitude larger than that achievable with the Moon. For this reason no mission or system requirements on this observation scenario are foreseen. Planets acquisition could nevertheless be attempted to show the platform capability to acquire them. Images would be then downlinked for processing and eventually test on/ground the navigation algorithms [13]. It is worth noting that while these kinds of measurements might not be sufficiently accurate for navigation around a celestial body, they could be exploited during interplanetary transfers [14].

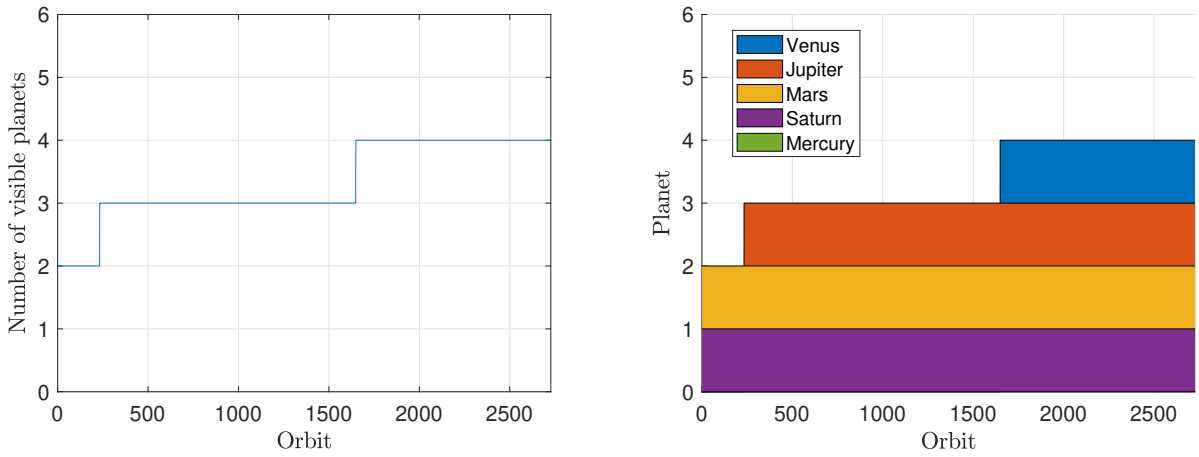

(a) Number of visible planets per orbit.

(b) Visible planets per orbit.

Figure 5: Planets visibility analysis

4 ON-BOARD AUTONOMOUS NAVIGATION

The characterization of the orbital regime and of the targets observation conditions are used to analyze and estimate the expected navigation filter performances. The main outcomes of this analysis are presented in this section.

The main modeling assumptions and the reasons behind the choice of a Hybrid Extended Kalman Filter (HEKF) are discussed in the following. The dynamics in a LEO orbit is well known and predictable due to continuous monitoring of conditions around Earth. Of course, the on-board navigation filter shall also comply with the limitations imposed by the available computational power and OBC performance. Therefore it is not possible to implement a complete, accurate orbital dynamics but it is rather necessary to determine the contributions and perturbations that are more relevant for the nominal orbital regime, to guarantee that the desired reconstruction accuracy will be met. The following assumptions are considered for the filter performance analysis:

- The satellite dynamics is modeled in order to catch the dominant perturbing accelerations acting on the operative LEO orbit, namely J2 and drag.
- The density model at 600 km is assumed constant to reduce system nonlinearity.
- The nominal SSO derived from mission analysis is considered the “true trajectory” to compare and test navigation performance.

During the Phase A study, the Hybrid Extended Kalman Filter has been selected as the navigation algorithm for this analysis because it is easy, lightweight, and it performs better than the classical Extended Kalman Filter (EKF) [4]. The filter implementation returns the spacecraft position in an Earth-Centered Inertial (ECI) frame, and linearized equations are used in this first stage. The latter point motivates also why second-order schemes are avoided. The general dynamics and sensor system equations in ECI frame can be summarized as:

$$\begin{cases} \ddot{\mathbf{r}} = -\frac{\mu}{\mathbf{r^3}}\mathbf{r} + \mathbf{p} + \mathbf{w} \\ \mathbf{y} = \mathbf{r} + \mathbf{n} \end{cases} \tag{1}$$

where μ is the Earth gravitational parameter, $\mathbf{r}$ is the satellite position vector, $\mathbf{p}$ is the perturbing acceleration vector acting on the spacecraft, and $\mathbf{w}$ and $\mathbf{n}$ are zero-mean Gaussian white noise vectors

capable to catch unmodeled accelerations (or equivalently wrong system parameters) and describe measurement uncertainty, respectively.
The navigation filter preliminary architecture is shown in Figure 6. As depicted, the inputs for the filter are the state $\mathbf{x_i}$ and time t_i, which are continuously updated depending on the propagation step, together with the uncertain position vector $\mathbf{r_{CF_U}}(t)$ representing the output of the Image Processing (IP) step. Since the image processing pipeline will be detailed during the Phase B study, its value was estimated by perturbing the ideal camera frame position $\mathbf{r_{CF_I}}(t)$ with different errors σ depending on the navigation scenario at hand. Specifically, 1σ errors of $(7.2 \times 7.2 \times 40)$ km for images of the Earth, and $(1000 \times 1000 \times 1000)$ km for those of Moon. These worst-case values were estimated according to the image processing performances available from literature.

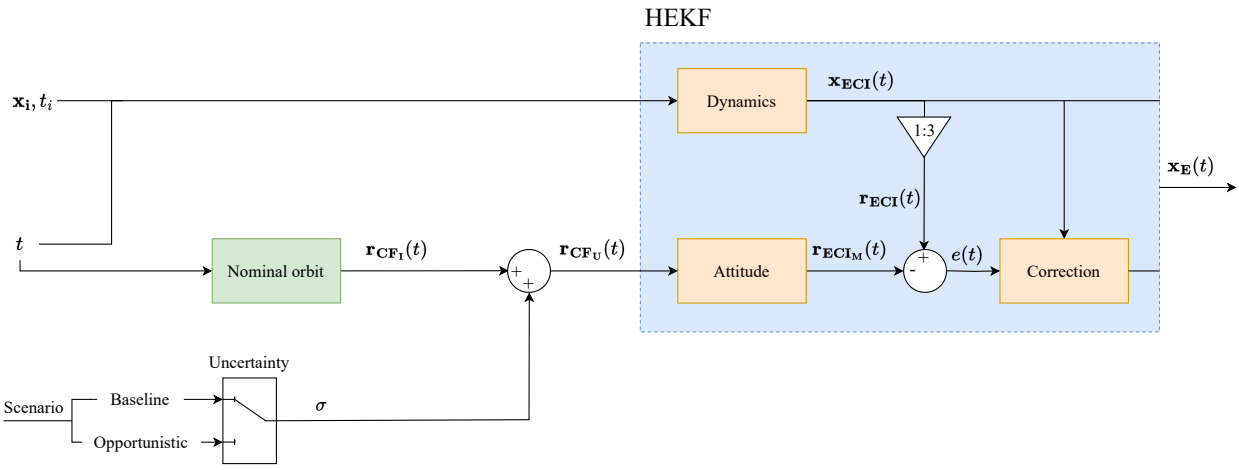

Figure 6: Navigation filter preliminary architecture. The blue rectangle groups the on-board filter building blocks, while the green box represents the generation of the IP output according to the actual (nominal) orbit. The scenario block instead represents the switch between observation mode defined by the OBC and the association of the uncertainty level to the measurement obtained with the IP.

Three different main blocks are reported in the HEKF module. The *Dynamics* block is the one devoted to the propagation of the initial state, and the estimation of the satellite state in ECI frame, in terms of position and velocity. It is worth noting that the propagation never stops, and continuously updates the current orbital knowledge even when no measurements are available (for simplicity, the loop was not closed in the Figure). Therefore, when no relevant surface features are detectable, this is the only working element, because no input from the image processing block is available. Conversely, when a measurement from the IP is available the *Attitude* block will convert the position vector from camera frame to the ECI. Once the measured position in ECI frame $\mathbf{r_{ECI_M}}(t)$ is available, it can be subtracted from the propagated position vector $\mathbf{r_{ECI}}(t)$ to obtain the so-called innovation error $\mathbf{e}(t)$. The last step consists of the *Correction* block in which from the propagated state, the Kalman filter gain K_f, and the innovation error, the final estimated state $\mathbf{x_E}(t)$ is retrieved:

$$\mathbf{x_E}(t) = \mathbf{x_{ECI}}(t) + K_f \mathbf{e}(t) \tag{2}$$

The simulation time has been limited to 1 day in order to check and reach Kalman filter convergence. Moreover, a tuning campaign has been performed to properly set filter parameters in terms of initial covariance matrices associated to state estimation error and process noise. This tuning is needed to have the state estimation error always inside the 3σ filter bounds and to try to catch the unmodeled

accelerations acting on the CubeSat. The HEKF 1σ performances are reported in Table 7 for the nominal scenario, and in Table 8 for the opportunistic one. In addition, as shown in the tables, both scenarios have been tested with different working sensor frequencies, represented by the elapsed time between two consecutive measurement update events.

Table 7: Filtering accuracy using Earth images (1σ sensor = $7.2 \times 7.2 \times 40$ km).

Measurement update time [min]	1σ **position [km]**	1σ **velocity [km/s]**
0.5	3	0.005
1	4.7	0.007
5	6.7	0.01
10	10	0.03
15	16	0.09

Table 8: Filtering accuracy using Moon images (1σ sensor = $1000 \times 1000 \times 1000$ km).

Measurement update time [min]	1σ **position [km]**	1σ **velocity [km/s]**
1	90	0.076
5	386	0.291
10	630	0.600
15	800	0.900

From the results shown, it can be noted how the filtering performance degrades when the time between two consecutive measurements increases. Moreover, when the frequency of 1 image every 15 minutes is exceeded, the filter uncertainty on the state estimation starts to tend to the sensor one. Therefore, above such frequency, the filtering brings limited benefits and the position error after estimation remains at the same level of the measurement noise. From this analysis, it is possible to select a functioning acquisition frequency according to the desired onboard navigation accuracy.
While the above analysis provides useful insight on the filter performances at converges, it gives limited or no information on the "dynamical" behaviour of the filter in-orbit. During the nominal mission operations, the satellite might experience periods with no target visibility or shall process different sequence of measurements. For this reason, it is necessary to study the actual filter performances and behaviour of the uncertainty associated to the state estimation in more detail for different measurement scenario. The underlying objective is to assess the capability of the filter to converge to the desired level of accuracy after the visibility gaps identified in Section 3.1.
The following 2 scenarios have been considered:

- **Scenario A**: no measurements are available during a no visibility interval of time t_1. This scenario simulates the navigation filter's not using measurement updates if the spacecraft is passing over a featureless region.
- **Scenario B**: opportunistic scenario with the usage of the IP on Moon images every minute for an entire orbit.

As reported in Table 6, a maximum no visibility time $t_1 = 180.5$ min has been set. Both cases consider a final time observability window $t_2 = 5$ min where Earth images can come in with a frequency $f_1 = 2$ images/min or $f_2 = 1$ images/min affecting the evolution of the covariance only along t_2 (using a higher sensor frequency, the final 3σ reached by the filter would be narrower). In all cases, the final 3σ position accuracy reached by the filter at the end of t_2 is ≈ 10 km using f_2, and ≈ 7 km using f_1.

In Figure 7, Scenario A results are shown considering f_2 as image frequency acquisition. The position uncertainty is reported in LVLH frame, whose X-axis is in the along-track direction, Y-axis in the normal-to-plane direction, and Z-axis in the radial direction. In this scenario, the maximum peak in 3σ error is ≈ 160 km.

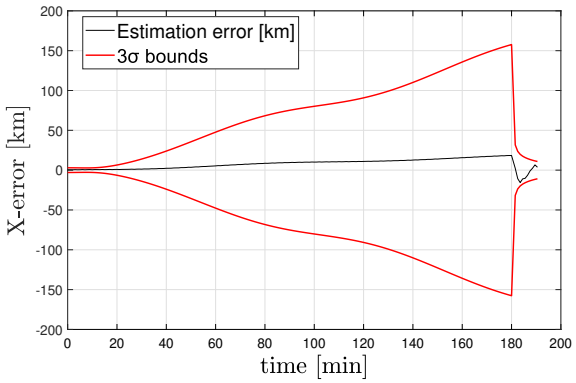

(a) Along-Track direction.

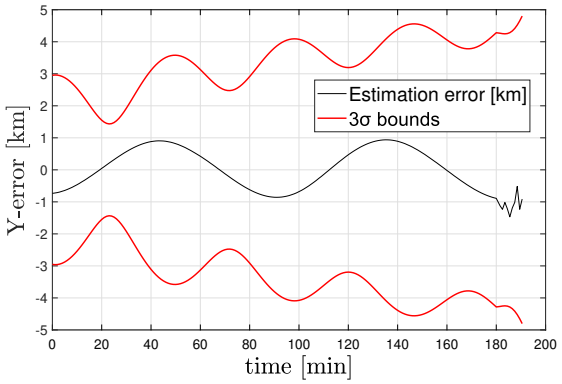

(b) Orbital angular momentum direction.

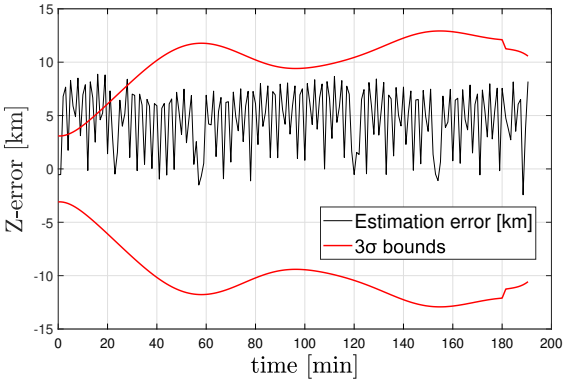

(c) Radial direction.

Figure 7: Scenario A, covariance evolution relative to satellite position in LVLH frame.

In Figure 8, the covariance evolution is shown considering Scenario B with a final f_2 as image frequency. For this scenario, the maximum peak reached in 3σ is ≈ 85 km at the end of the orbital time. From this analysis it can be deduced that, inserting sensor measurements obtained from Moon observations, i.e., with uncertainty of 1000 km, the covariance evolution remains similar to Scenario A without improving significantly the covariance divergence peak in short terms.
To conclude, it is worthy to highlight how this preliminary analysis has been done using simple models and filter algorithm (HEKF) in order to obtain an overall idea of possible state filtering performances achievable on the target orbit. Further analyses will be performed in Phase B, with the aim of assessing the performances of different filters, like the Unscented Kalman Filter (UKF) [2], [3]. In addition, more refined dynamical models (e.g., introducing SRP) could be introduced to determine which set of modeled perturbation gives the more reliable and accurate results.

5 CONCLUSION

In this work a generic overview of the FUTURE mission is provided together with a detailed description of its mission analysis and on-board navigation filter. Preliminary results of the navigation filter are reported both for the nominal and for the opportunistic scenario in order to assess its performance.

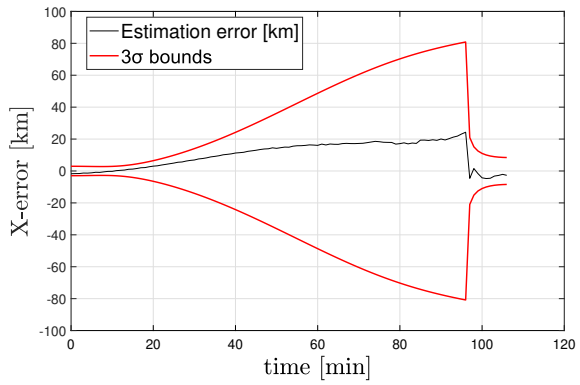

(a) Along-Track direction.

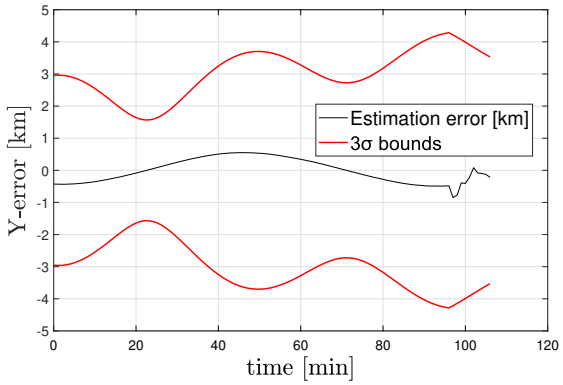

(b) Orbital angular momentum direction.

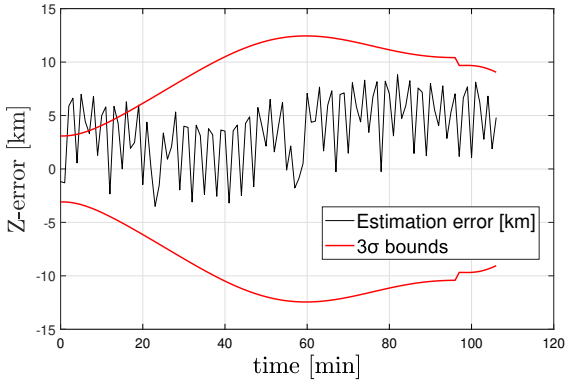

(c) Radial direction.

Figure 8: Scenario B, covariance evolution relative to satellite position in LVLH frame.

The achievable 1σ accuracy of 3 km in position with a update frequency of 30 s: this value is represent a worst-case scenario since the dynamics model used could be improved and the error estimation is based on conservative values extracted from literature. For this reason, other filter implementations will be assessed during the next mission study phases which might produce an increase in navigation performances. It is also important to highlight that while the overall performances is clearly lower than the one of a GNSS system (which could reach a sub-meter level accuracy in position), it could anyway be already sufficient when orbiting around other celestial bodies, especially since it could be possible to obtain those estimates directly and regularly on board with no need to wait from an update from ground. In those cases, the lack of oceans, the absence of dense atmosphere, and the richness of constant morphological features such as craters and big boulders would produce a more favourable scenario than that experienced by Earth-orbiting satellites.

For what concerns the opportunistic scenarios, it has been observed that these are producing only limited benefits in the overall navigation performance, mainly due to the high uncertainty estimated for the outputs of the IP of Moon images. First it is worth observing that the analysis reported here are considering only one orbital revolution: for longer gaps with no landmark visibility these measurements would anyway start to become effective and at least mitigate the uncertainty growth. Also in this case further analysis are foreseen after the whole IP process has been detailed and algorithms for Moon detection and Line-of-Sight extraction selected. These are indeed prerequisites for a more refined estimation of the error-chain and actual noise level to be associated to the measurements produced by the AI-based image processing.

The studies and analysis presented in this work will be further developed during the Phase B of FU-

TURE. The main challenges for the immediate future are the consolidation of the navigation strategy and its implementation in a software-in-the-loop and hardware-in-the-loop scenario.

6 ACKNOWLEDGMENTS

The work described in this paper was carried out as part of ASI's ALCOR program under contract No. 2022-17-I.0 for the Phase A study of the mission FUTURE: Fully aUtonomous feaTUre Recognition planetary Explorer. The authors would like to acknowledge the support received by the whole FUTURE consortium, which is led by Tyvak International, and by the ASI team.

REFERENCES

[1] R. E. Kalman, "A new approach to linear filtering and prediction problems," *Journal of Fluids Engineering*, vol. 82, no. 1, pp. 35–45, 1960. DOI: 10.1115/1.3662552.

[2] S. J. Julier and J. K. Uhlmann, "New extension of the kalman filter to nonlinear systems," in *Signal processing, sensor fusion, and target recognition VI*, vol. 3068, 1997, pp. 182–193.

[3] E. A. Wan and R. Van Der Merwe, "The unscented kalman filter for nonlinear estimation," in *Proceedings of the IEEE 2000 Adaptive Systems for Signal Processing, Communications, and Control Symposium*, 2000, pp. 153–158. DOI: 10.1109/ASSPCC.2000.882463.

[4] D. Simon, *Optimal state estimation: Kalman,* H_∞*, and nonlinear approaches*. 2006, vol. 10.

[5] J. J. Wang, "Antennas for global navigation satellite system (gnss)," *Proceedings of the IEEE*, vol. 100, no. 7, pp. 2349–2355, 2012.

[6] J. A. Christian, "Optical navigation using planet's centroid and apparent diameter in image," *Journal of guidance, control, and dynamics*, vol. 38, no. 2, pp. 192–204, 2015. DOI: 10.2514/1.G000872.

[7] M. Straub and J. A. Christian, "Autonomous optical navigation for earth-observing satellites using coastline matching," in *AIAA Guidance, Navigation, and Control Conference*, 2015, p. 1334. DOI: 10.2514/6.2015-1334.

[8] J. A. Christian and S. B. Robinson, "Noniterative horizon-based optical navigation by cholesky factorization," *Journal of Guidance, Control, and Dynamics*, vol. 39, no. 12, pp. 2757–2765, 2016. DOI: 10.2514/1.G000539.

[9] B. Maass, "Robust approximation of image illumination direction in a segmentation-based crater detection algorithm for spacecraft navigation," *CEAS Space Journal*, vol. 8, pp. 303–314, 2016. DOI: 10.1007/s12567-016-0129-1.

[10] D. Mortari, C. N. D'Souza, and R. Zanetti, "Image processing of illuminated ellipsoid," *Journal of Spacecraft and Rockets*, vol. 53, no. 3, pp. 448–456, 2016. DOI: 10.2514/1.A33342.

[11] J. A. Christian, "A tutorial on horizon-based optical navigation and attitude determination with space imaging systems," *IEEE Access*, vol. 9, pp. 19 819–19 853, 2021. DOI: 10.1109/ACCESS.2021.3051914.

[12] V. Franzese, F. Topputo, F. Ankersen, and R. Walker, "Deep-space optical navigation for m-argo mission," *The Journal of the Astronautical Sciences*, vol. 68, pp. 1034–1055, 2021. DOI: 10.1007/s40295-021-00286-9.

[13] E. Andreis, P. Panicucci, V. Franzese, and F. Topputo, "A Robust Image Processing Pipeline for Planets Line-Of-sign Extraction for Deep-Space Autonomous Cubesats Navigation," in *44th AAS Guidance, Navigation and Control Conference*, 2022, pp. 1–19.

[14] E. Andreis, V. Franzese, and F. Topputo, "Onboard Orbit Determination for Deep-Space CubeSats," *Journal of Guidance, Control, and Dynamics*, pp. 1–14, 2022.

[15] G. Leccese, A. Fedele, and S. Natalucci, "Overview and roadmap of italian space agency activities in the micro- and nano-satellite domain," in *73rd International Astronautical Congress (IAC)*, 2022.

[16] E. Turan, S. Speretta, and E. Gill, "Autonomous navigation for deep space small satellites: Scientific and technological advances," *Acta Astronautica*, 2022.

[17] V. Franzese and F. Topputo, "Celestial bodies far-range detection with deep-space cubesats," *Sensors*, vol. 23, no. 9, 2023. DOI: 10.3390/s23094544.